SANDIA REPORT
SAND2013-9513
Unlimited Release
Printed November 2013

Technology for On-Chip Qubit Control with Microfabricated Surface Ion Traps

Clark Highstrete, Sean Scott, Jonathan D. Sterk, Edwin J. Heller, Peter Maunz, Christopher D. Nordquist, James E. Stevens, Chris P. Tigges, and Matthew G. Blain

Prepared by Clark Highstrete
Sandia National Laboratories
Albuquerque, New Mexico 87185

Sandia National Laboratories is a multi-program laboratory managed and operated by Sandia Corporation, a wholly owned subsidiary of Lockheed Martin Corporation, for the U.S. Department of Energy's National Nuclear Security Administration under contract DE-AC04-94AL85000.

Approved for public release; further dissemination unlimited.

Sandia National Laboratories

Issued by Sandia National Laboratories, operated for the United States Department of Energy by Sandia Corporation.

Printed in the United States of America. This report has been reproduced directly from the best available copy.

Available to DOE and DOE contractors from
U.S. Department of Energy
Office of Scientific and Technical Information
P.O. Box 62
Oak Ridge, TN 37831

Telephone: (865) 576-8401
Facsimile: (865) 576-5728
E-Mail: reports@adonis.osti.gov
Online ordering: http://www.osti.gov/bridge

Available to the public from
U.S. Department of Commerce
National Technical Information Service
5285 Port Royal Rd.
Springfield, VA 22161

Telephone: (800) 553-6847
Facsimile: (703) 605-6900
E-Mail: orders@ntis.fedworld.gov
Online order: http://www.ntis.gov/help/ordermethods.asp?loc=7-4-0#online

SAND2013-9513
Unlimited Release
Printed November 2013

Technology for On-Chip Qubit Control with Microfabricated Surface Ion Traps

Clark Highstrete
Quantum Information Sciences Department (5643)

Sean Scott and Christopher D. Nordquist
RF/Optoelectronics Department (1742)

Jonathan D. Sterk, Peter Maunz, Chris P. Tigges, and Matthew G. Blain
Photonic Microsystem Technologies Department (1725)

Edwin J. Heller
Microsystems Integration Department (1718)

James E. Stevens
MESAFab Operations 2 Department (1747)

Sandia National Laboratories
P.O. Box 5800
Albuquerque, New Mexico 87185

Abstract

Trapped atomic ions are a leading physical system for quantum information processing. However, scalability and operational fidelity remain limiting technical issues often associated with optical qubit control. One promising approach is to develop on-chip microwave electronic control of ion qubits based on the atomic hyperfine interaction. This project developed expertise and capabilities at Sandia toward on-chip electronic qubit control in a scalable architecture. The project developed a foundation of laboratory capabilities, including trapping the $^{171}Yb^{+}$ hyperfine ion qubit and developing an experimental microwave coherent control capability. Additionally, the project investigated the integration of microwave device elements with surface ion traps utilizing Sandia's state-of-the-art MEMS microfabrication processing. This effort culminated in a device design for a multi-purpose ion trap experimental platform for investigating on-chip microwave qubit control, laying the groundwork for further funded R&D to develop on-chip microwave qubit control in an architecture that is suitable to engineering development.

Acknowledgments

This work was funded under LDRD project number 154195, entitled "On-Chip Coherent Qubit Operations with Microfabricated Surface Ion Traps."

Contents

Figures

Tables

Nomenclature

AOM	acousto-optic modulator
CQO	coherent qubit operation
dB	decibel
DOE	Department of Energy
EOM	electro-optic modulator
PBS	polarizing beam splitter
QIP	quantum information processing
SNL	Sandia National Laboratories

1 Introduction

1.1 Overview

Quantum information processing promises to perform some significant tasks far more efficiently than can be accomplished classically. Important examples of possible applications include quantum computation, quantum simulation, and quantum communication. Trapped atomic ions are a leading physical system for quantum information processing. However, while all the requirements for quantum information processing have been demonstrated at the proof-of-principle level in trapped ion systems, scalability and operational fidelity remain as the limiting technical issues.

To date, laser systems have been primarily used to manipulate ion quantum bits (qubits). However, the complexity and power requirements of laser systems severely limit scalability. Technical difficulties with laser stability and fundamental limits on coherence for optically controlled ion qubits due to atomic spontaneous emission have also kept operational fidelities below fault tolerant levels, and are likely to remain a limiting factor for the foreseeable future. A solution to the limitations posed by lasers is to use microwave fields generated by simple, highly stable, and commercially available sources to control ion qubits. Microwaves can be used to manipulate qubits that are by nature practically immune to decoherence by spontaneous emission, thus significantly improving operational fidelity. Laser-less operation also reduces the power requirements of a quantum computer, addressing a practical limitation of trapped-ion quantum information processing.

So far, limited progress has been realized with this approach because, for free space microwave radiation, the relatively long wavelength: (1) precludes tight focusing thus causing all qubits to be addressed simultaneously and (2) small field gradients on the atomic scale produce negligible coupling to inter-atomic motional modes used for qubit gates. However, utilizing Sandia's state-of-the-art microfabrication techniques, microwave electrodes with sub-wavelength dimensions can be designed to localize the fields and generate the high magnetic field gradients required for quantum information processing.

This project developed expertise and capabilities at Sandia toward on-chip, localized, and laser-less qubit operations in a scalable architecture. The project developed a foundation of basic building blocks, including laboratory capabilities for hyperfine ion qubit trapping, coherent control, and experimentation. Additionally, the project investigated the integration of simple microwave device elements with surface ion traps utilizing Sandia's state-of-the-art MEMS microfabrication processing. This effort culminated in a device design for a multi-purpose ion trap experimental platform for investigating on-chip microwave qubit control. Overall, this work has laid the groundwork for further funded R&D to develop on-chip microwave qubit control in an architecture that is suitable to engineering development.

1.2 Background

1.2.1 Ion qubits

Trapped atomic ion quantum bits (qubits) have been employed successfully for quantum information processing (QIP) and are a promising physical qubit candidate for developing quantum computation.[1, 2] Individual qubits are defined by isolating two quantized energy levels of the ion's configuration. Different states can include configurations of various properties of the atomic electron and nucleus such as electron orbit, electron spin, and nuclear spin. However, since the state of the electron is always involved, it is convenient to refer to them as *electronic states* and transitions between them as *electronic transitions*. These quantum electronic states can be separated by energy differences corresponding to electromagnetic excitation from radio frequencies (RF) to optical wavelengths. Controlled electronic transitions are performed by applying pulses of electromagnetic fields at the corresponding frequency/wavelength (*excitation pulses*).

1.2.2 Quantum operations

There are two important types of operations carried out in quantum information processing with trapped ions. First, manipulation of an individual ion to control its electronic quantum state configuration, as mentioned above, is known as a *single qubit rotation*. This term refers to the mathematical rotation of the quantum state vector in the Bloch-sphere [3] representation and is analogous to the rotation of the spin vector in Nuclear Magnetic Resonance (NMR). Additionally, trapped ions can be made sufficiently cold (i.e. their motion sufficiently suppressed by, for instance, laser cooling) so that the state of their motion may also be described quantum mechanically. Ion motion is then described by quantized levels of excitation (energy levels) of a quantum harmonic oscillator. Using excitation pulses tuned to the electronic transition plus or minus the harmonic-oscillator energy level spacing, changes in the ion's electronic state configuration can be coupled to changes in its amount of harmonic oscillator motional excitation, either increasing or decreasing its motional energy. With single or multiple qubits, excitation of these motional modes requires significant electromagnetic field gradients on the scale of the ion motion, which is typically on the order of 10 nm. [4, 5]

For quantum information processing, it is necessary to interact ions together in order to perform processing operations with the information stored in the different qubits, similar to performing logic operations with different bits in a classical computer. The primary means of doing this is to trap ions together in a linear chain, so that they are separated by, and interact through, their electrostatic (Coulomb) repulsion. Then, instead of single ion harmonic oscillator motional excitations, there are collective modes of oscillation for all of the ions. Two simple examples are: (1) the *center of mass* (COM) mode for two ions, where they move jointly side to side, and (2) the *stretch* mode, where the ions oscillate towards and away from each other. By tuning excitation pulses to an ion's electronic state transition plus or minus the oscillation mode energy level spacing, changes in an ion's electronic state configuration are coupled to changes in the amount of motional excitation in that mode. Because this excitation involves other ions, exciting their motion as well, the overall (electronic + motional) quantum states of the various ions interact and their quantum states become *entangled*.

Because of this entanglement, the occurrence of a quantum transition involving multiple ions in response to an electromagnetic pulse, can be made conditional on the initial states of the qubits, thus enabling quantum logic operations. Controlled interactions of this sort between qubits are the second operation necessary to perform quantum information processing and are known as *multi-qubit gates,* analogous to gate operations with multiple bits in classical computation. [1, 5, 6]

1.2.3 Methods for qubit manipulation

To date, qubit rotations and gates are performed primarily with tightly focused laser beams. This is done either with direct excitation of electronic energy levels separated by energies corresponding to optical wavelengths (*optical qubits*) or indirectly with simulated Raman transitions, where two laser beams are applied at wavelengths/frequencies that are separated by the required transition frequency.[5] Raman transitions are normally used with the electronic states defined by the hyperfine interaction between the atomic nucleus and the electron in odd-isotope atoms (i.e. with net nuclear spin). This interaction causes an energy splitting of the electronic ground state into multiple levels which are separated by energies corresponding to microwave frequencies. These qubits are commonly known as *hyperfine qubits* or, alternatively, *clock states* because of their widespread use in atomic-clock applications.

Most current schemes for quantum information processing with trapped ions use laser-induced interactions to implement the necessary qubit rotations and gates with one-dimensional chains of trapped ions. While laser-based schemes have been successful in manipulating small numbers of ions, scaling up to larger register sizes and/or multiple quantum registers will, however, require a large overhead in laser-beam power and control. Additionally, multi-qubit gates rely on the ability to spectrally isolate a single motional mode of an ion chain. Because there are $3N$ modes of motion for N trapped ions, as N becomes large the mode spectrum becomes so dense that the gate speeds must be significantly reduced to avoid off-resonant coupling to other modes.[2] Reduction of gate speeds is highly detrimental to quantum computing because decoherence of the qubits in time limits the fidelity of the operations. As a result, large numbers of qubits must be dedicated to performing error correction, thus escalating critical system resource requirements.

The alternative to 1D ion chains is to distribute the ion qubits in an array of multiple trap zones.[7] In this architecture, gate operations can be carried out on a relatively small number of ions in multiple processing zones. Interactions are facilitated by physically moving the ions to different zones for different operations in a “Quantum CCD bus” architecture, analogous to movement of charges on a solid-state CCD image sensor. Yet, even in this architecture, optical qubits require laser beams to be applied in several locations simultaneously for parallel operations. Moreover, spontaneous emission and technical difficulties associated with stabilizing laser frequency, phase, amplitude, and beam pointing have kept optical qubit gate fidelities below fault tolerant levels and are likely to remain a limiting factor for the foreseeable future.[2]

1.2.4 Use of microwaves

The shortcomings of lasers for qubit operations can be overcome by using instead *microwave* magnetic fields to *directly* manipulate hyperfine qubits. These clock states are commonly used for atomic frequency standards because they are highly stable; they are practically immune to decoherence by spontaneous emission and are readily addressed by highly stable, commercial-off-the-shelf (COTS) microwave sources. To date, the advantages of using microwave magnetic fields have not been realized because *for free-space microwaves*, their long wavelength precludes focusing, causing all qubits to be simultaneously addressed, and only negligible field gradients can be produced on the ion-motion scale, precluding coupling to motional modes.[5] To overcome these issues, microfabricated ion traps offer a solution: microwave electrodes with sub-wavelength dimensions can localize fields to individually address subsets of qubits and generate sufficient magnetic field gradients to excite entangling motional modes [5, 8-10].

1.2.5 Toward a microwave qubit quantum-information processor

Ultimately, a quantum-information processor based on microwave manipulation of qubits would need to have electromagnetically isolated regions where qubit preparations and interactions are accomplished with microwave fields delivered with on-chip waveguides. The primary technical challenges include: (1) integrating high magnetic field gradients and microwaves on-chip with effective field localization, involving relatively high current densities to provide sufficient field strength / gradients; and (2) shielding or cancelling of microwave fields from other zones to minimize unintentional qubit manipulations due to cross-talk (*witnessing* or *spectator* effects). These challenges are uniquely suited to Sandia's device integration capabilities and demonstrated experience in modeling, designing, microfabrication, and implementation of surface ion traps.

1.2.6 Significance

Published studies that consider the requirements for building a quantum information processor focus on critical technology benchmarks but do not consider the likely cost.[11] Following the blueprint article of Steane, we estimate this cost both for a QIP based on laser control of qubits and a QIP based on microwave control of qubits. Table 1 shows the essential elements for either approach. We estimate that the elimination of sophisticated, ultra-stable laser sources from a quantum information processor that would outperform a classical computer results in a 700-fold reduction in cost.

The quantum computer architecture analyzed by Steane requires 1,000 operations in parallel. The costs listed in Table 1 account for that factor. A notable point in this comparison is that the components necessary for microwave qubit control are available "commercial off-the-shelf" (COTS), whereas the laser specifications require custom development. For example, a frequency source is available from Symmetricom and microwave pulses can be generated using direct digital synthesizers (DDS) controlled by field-programmable gate arrays (FPGA) from Xilinx or Analog Devices.

Qubit control	Pointing stability		Intensity stability		Frequency stability		Power		Total cost
	Value	Cost	Value	Cost	Value	Cost	Value	Cost	
Lasers	**1 µm**	**Min.**	**10^{-8}**	**Incl.**	**10^{-10}**	**$500M**	**2.3 kW**	**$300M**	**$800,000,000**
Microwaves	**N/A**	**0**	**N/A**	**0**	**10^{-11}**	**$0.1M**	**COTS**	**$1M**	**$1,100,000**

Table 1: Cost comparison of implementing a quantum information processor with laser control of qubits vs. microwave control of qubits. COTS: "commercial off the shelf;" Min.: "Minimal;" Incl.: "Included." Notes: The laser frequency-stability cost includes the cost of acousto-optic and electro-optic modulators needed for frequency agility. There is no COTS product that meets the required laser frequency stability. The laser power specification is based on numbers reported in reference [12]. The cost of lasers is based on the use of ytterbium and accounts for state-of-the-art quadrupled fiber lasers that offer the highest output radiant power at the lowest cost.

1.2.7 Status of research and development

Research in this area has been limited. The use of static magnetic fields to isolate qubits in frequency space and perform qubit gates has been proposed.[8] However, results have been limited to RF Zeeman transitions in a macroscopic trap [13] and optical transitions in a microfabricated surface ion trap.[14] Alternatively, a promising new direction is to use magnetic field gradients oscillating at microwave frequencies to perform gates.[9] Significant efforts in this direction also exist in the National Institute of Standards and Technology (NIST) Ion Storage Group and the Oxford Ion Trap Quantum Computing group, both of which are current collaborators with Sandia.

To date, the leader in the field is the NIST group, having recently demonstrated two-qubit coherent operations with magnetic field gradients oscillating at microwave frequencies.[15] NIST has also recently demonstrated single qubit rotations with fidelity in the range required for fault tolerant quantum computing.[16] However, the NIST approach is confined to devices with only surface electrodes, which limits the type of structure that can be used to generate magnetic fields and gradients, requiring excessively large microwave currents and hence impractically large cross section interconnects. Additionally, this technology limits allowable qubit transition frequencies because of skin-depth issues. Finally, having all microwave transmission lines on the surface allows microwave fields to permeate all regions of the device due to lack of shielding and the fact that the fields due to transmission lines fall off

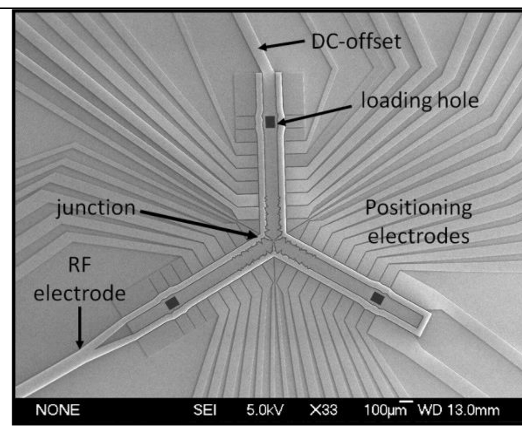

Figure 1.1: Sandia Y junction microfabricated surface ion trap used to investigate ion shuttling through a junction of multiple trap linear segments (the "arms" of the Y). Ions are initially trapped at the loading hole (a lithographically defined and backside etched through hole) then shuttled using positioning electrodes to arbitrary locations along the Y arms.

weakly with distance. All of these challenges need to be answered in order to advance this concept from proof-of-principle experiment to scalable technology.

The Sandia team has a history of successful research and development in microfabricated ion traps and atomic physics using these devices. Sandia's ion trapping achievements include developing microfabricated surface ion traps with unprecedented reproducibility [17, 18], demonstrating the first highly repeatable through-junction shuttling in a surface trap (Figure 1.1),[18] integrating fluorescence collection optics with a microfabricated surface ion trap,[19] and developing an ion trap with all electrodes connected beneath a top metal layer by Tungsten vias (Figure 1.2). Sandia successfully demonstrated 3 million arm-to-arm junction traverses with a single ion – a world record by a factor of over 100,000. Other firsts were placing by shuttling three ions into separate arms simultaneously, and trapping two ions together in a single harmonic potential well, separating them, shuttling into separate arms, and rejoining them in the original location in reversed order. Sandia traps created under these projects are now being used by leading research institutions such as the Joint Quantum Institute (JQI) at the University of Maryland, NIST/Boulder, Duke University, Georgia Institute of Technology, and Oxford University.[20] However, prior to this project, Sandia had no coherent qubit control capability in the laboratory and no development of on chip microwave capability for qubit control.

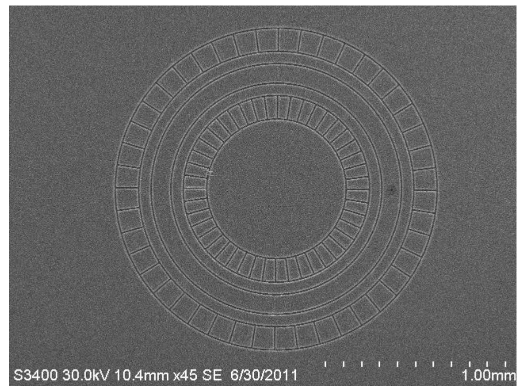

Figure 1.2: A Sandia ring-shaped ion trap. This trap topology is only feasible using a 4-metal-layer microfabrication process, due to electrode cross-overs. Sandia is the only place where ion traps are fabricated with this process.

1.3 Project scope

The objective of this project was to develop expertise and capabilities at Sandia toward on-chip, localized, and laser-less qubit operations in a scalable architecture. The initial project goals addressed three areas: (1) development and implementation of hyperfine ion qubit trapping, coherent control, and experimentation capabilities in the laboratory with legacy ion trap devices and external microwave sources, (2) design of basic on-chip microwave control test structures, and (3) implementation of these test structures in the laboratory.

Over the course of the project, the scope shifted from implementing legacy devices and design/implementation of basic structures to development of laboratory capabilities and design studies of more sophisticated devices. Extensive modeling studies were accomplished to investigate the feasibility of on-chip microwave devices for laser-less ion qubit control. Studies have identified device designs to supply adequate magnetic fields within manufacturing constraints. Additionally, passive minimization of qubit zone cross-talk and active cancellation with multiple electrode control degrees of freedom has been studied. Code was written to calculate magnetic fields and gradients of surface coil elements and to simultaneously solve for zero field solutions at ion position. Preliminary designs were identified that are capable of zeroing field at ions while providing large field gradients, two critical requirements for two-qubit gates.

Ultimately, the project developed a foundation of enabling building blocks. The project developed laboratory capabilities for hyperfine ion qubit trapping, coherent control, and experimentation. Additionally, the project investigated the integration of simple microwave device elements with surface ion traps utilizing Sandia's state-of-the-art MEMS microfabrication processing. This effort culminated in a device design for a multi-purpose ion trap experimental platform for investigating on-chip microwave qubit control. Overall, this work has laid the groundwork for further funded R&D to develop on-chip microwave qubit control in an architecture that is suitable to engineering development.

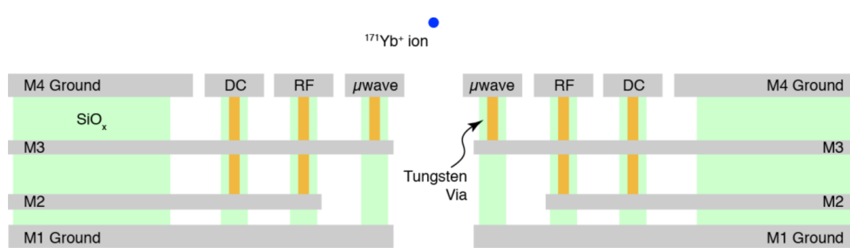

Figure 1.3: Schematic representation of Sandia's state-of-the-art 4-metal-layer microfabrication technology for ion traps. Metal layers (M1, M2, M3, M4) are separated by oxide (SiOx) pillars with tungsten (W) via interconnects. The precisely controlled M4 metal-layer overhangs shield ions from dielectric noise sources. DC and RF trap electrodes (M2) and microwave (M3) utilize buried metal lines with M4 top ground plane shielding fields on chip.

This project investigated the integration of simple microwave device elements with surface ion traps utilizing Sandia's state-of-the-art 4-metal-layer microfabrication process (Figure 2.3). The 4-metal-layer process is ideally suited because microwaves can be delivered by transmission lines shielded underneath a surface ground plane. Interaction regions involve local microwave electrodes; a top-side microwave ground plane covers the rest of the device, maximally shielding microwave fields from affecting other trap regions.

2 Laboratory capability development

This section describes the development of technical building block capabilities toward performing coherent quantum operations (CQO) and coherence measurements in the laboratory. Each CQO on the hyperfine qubit involves a precisely timed control process requiring ion trapping and laser cooling, optical state initialization, resonant microwave pulse application, and optical readout/measurement of the final qubit state. The capabilities to trap, cool, initialize, and read out the $^{171}Yb^{+}$ isotope was developed under this project. Additionally, the electronics for applying microwave pulses to manipulate the hyperfine qubit were developed as were extensive experimental control software for coherent control experiments. Although only the trapping and cooling capabilities were demonstrated under this project, the technology was transferred to new projects at Sandia. The next sections describe the optical, microwave, and control electronics and software components developed to enable coherent qubit operations (CQO) in the laboratory.

2.1 Optical components and operations

2.1.1 Laser and optical system

The optical capability to trap, cool, initialize, and read out the $^{171}Yb^{+}$ isotope was developed under this project from the simpler existing $^{174}Yb^{+}$ capability. The odd-isotope ytterbium ion $^{171}Yb^{+}$ allows for efficient preparation and detection of the ground state hyperfine levels.

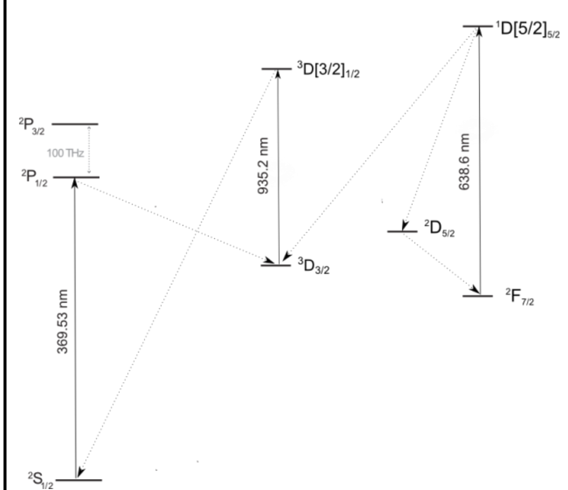

Figure 2.1: Partial energy level diagram of Yb^{+} with full scheme for ion trapping.[21] A 638.6 nm laser was not used for this project, which results only in occasional ion loss.

A partial energy diagram for Yb^{+} ions in general is shown in Figure 2.1, which indicates the relevant laser wavelengths. The $^{2}S_{1/2} \leftrightarrow {}^{2}P_{1/2}$ transition at 369.53 nm is used for Doppler-cooling and to observe ion fluorescence. The low-lying metastable $^{2}D_{3/2}$ state is depopulated by light at 935.2 nm resonant with the $^{2}D_{3/2} \leftrightarrow {}^{3}D[3/2]_{1/2}$ transition, which quickly returns the ion to the cooling transition. The ion only occasionally reaches the $^{2}F_{7/2}$ state, requiring light near 638.6 nm to return it to the cooling cycle. Existing lasers at 369.53 nm and 935.2 nm were utilized for this work. However, a laser at 638.6 nm was not available, but the occasional ion loss due to population trapping in the $^{2}F_{7/2}$ state was acceptable. [21]

With the required Ytterbium lasers in operation, the the optical system shown in Figure 2.2 was developed to address the additional atomic transitions required due to hyperfine energy level splittings of the odd isotope $^{171}Yb^{+}$ions (see 2.1.2 below). This system generates and controls beams of 369 nm light with sidebands at 2.1 GHz and 14.74 GHz. Two resonant electro-optic modulators (EOM) at 2.1 and 7.37 GHz add sidebands at 2.1 Gz and 14.74 GHz (second order) to the 369 beams. The system also provides the ability to independently switch three 369 nm sub-beams using the first order sidebands from RF driven acousto-optic modulators (AOM). Finally, it provides control of the relative beam intensities, and allows recombination of two beams, using custom 369 nm half-wave plates and polarizing beam splitter cubes (PBS). The resulting beams are designed to provide ion Doppler cooling for ion trapping, quantum state preparation, and quantum state detection as described in the following paragraphs. Similarly, a fiber EOM was added to the 935 nm beam to generate a 3.07 GHz sideband.

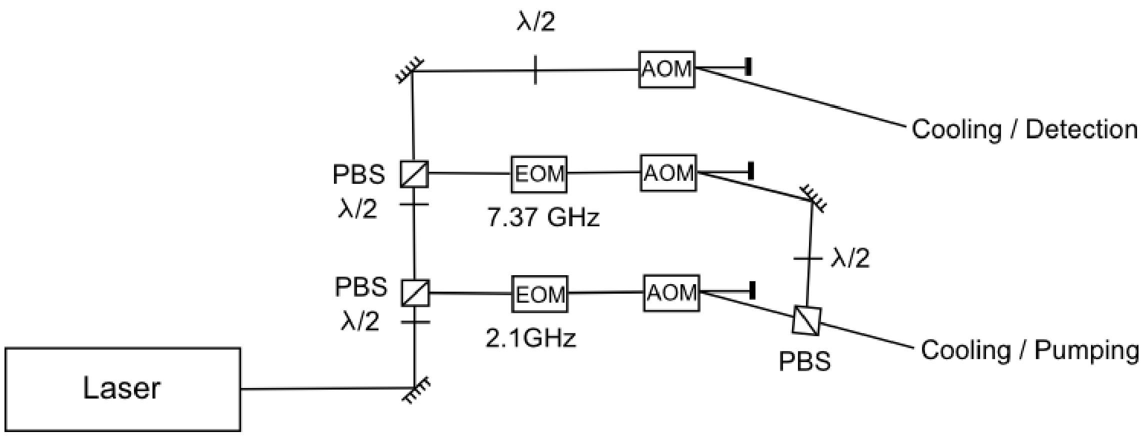

Figure 2.2: 369 nm optical setup for trapping and controlling $^{171}Yb^+$

2.1.2 Atomic structure and trapping of $^{171}Yb^+$ ions

As seen in Figure 2.3, the atomic hyperfine interaction breaks the energy degeneracy between the hyperfine levels of different total atomic angular momentum, F. To trap $^{171}Yb^+$, a DC magnetic field is applied, which defines a quantization axis and polarization reference. The applied magnetic field also results in Zeeman shifts of the various magnetic sublevels associated with a particular angular momentum, F. This splitting avoids coherent population trapping due to interference. These sublevels are designated by $m_{F,}$ which indicates the projection of the angular momentum along the quantization axis.

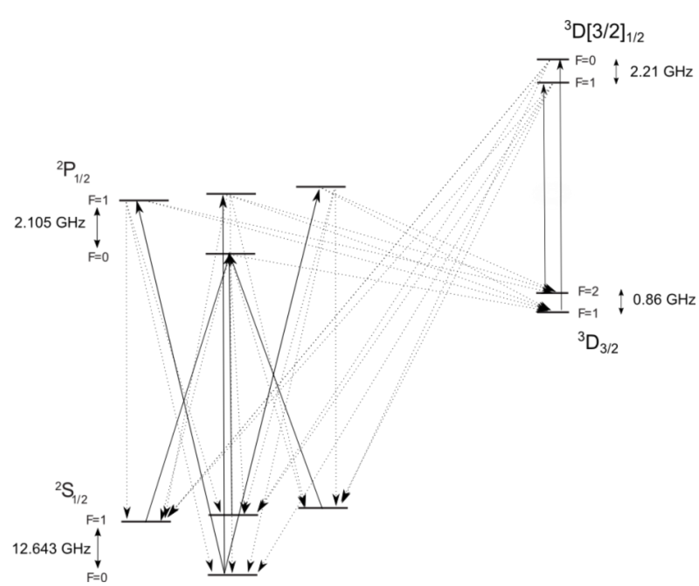

Figure 2.3: $^{171}Yb^+$partial level diagram and trapping scheme

The $^{171}Yb^+$ ion is Doppler cooled by light slightly red detuned from the $^2S_{1/2}$|F=1>↔$^2P_{1/2}$|F=0> transition at 369.53 nm. Off-resonant coupling to the $^2P_{1/2}$|F =1> manifold results in population trapping in |0>. To prevent this during cooling intervals, the 369.53 nm cooling beam is passed through an EOM driven at 7.37 GHz, as shown in Figure 2.2. The resulting second-order sideband is resonant with the $^2S_{1/2}$|F=0>↔$^2P_{1/2}$|F=1> transition, which returns the ion to the cooling cycle. Population trapping in the $^2D_{3/2}$|F=1> manifold is avoided by application of a laser at 935.2 nm, which rapidly returns the atom to the cooling cycle via the $^3D[3/2]_{1/2}$ |F=0> level. [21]

In order to trap $^{171}Yb^+$ in the laboratory, a DC magnetic field of approximately 5 Gauss was externally applied. Three-axis magnetic field control was provided by magnetic coils arranged in a quasi-Helmholtz configuration around the vacuum chamber viewports on the π and σ polarization axes as well as a single vertical trim coil around the top flange. Neutral atom fluorescence spectroscopy was performed to spectrally isolate the $^1S_0$ ↔ $^1P_1$ transition of the neutral ^{171}Yb isotope from the other Yb isotopes at 399 nm. Once this transition was identified, the 399 nm laser was tuned to the transition and two photon ionization was used to form $^{171}Yb^+$ ions. Figure 2.4 shows a fluorescence image of successful trapping of $^{171}Yb^+$ ions. This was the first demonstration of a capability to trap an ion species applicable as a hyperfine qubit at Sandia.

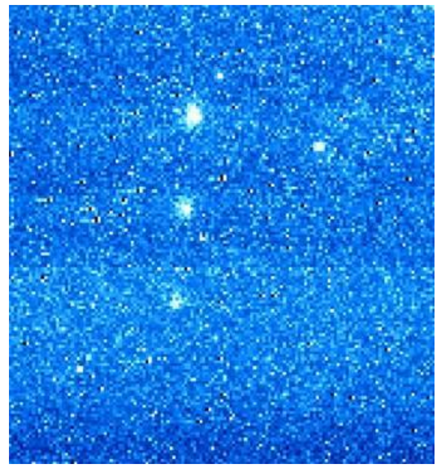

Figure 2.4: Fluorescence image of a 171Yb+ three-ion crystal.

2.1.3 $^{171}Yb^+$ qubit definition and state initialization

The applied magnetic field also serves to establish a quantization axis for the ion, allowing definition of the hyperfine qubit. As seen in Figure 2.5, the qubit is (arbitrarily) defined as the two first-order magnetic field-insensitive hyperfine levels of the $^2S_{1/2}$ ground state. The $^2S_{1/2}$|F=1,m_F=0> state is defined as the logical qubit state |1> , and the $^2S_{1/2}$|F=0,m_F=0> state was defined as |0>, where F is the total angular momentum of the atom and. The qubit states are separated by a frequency of 12 642 812 118.5±δ Hz, where δ = (310.8)B^2 is the second-order Zeeman shift, and B is the magnetic field in Gauss.

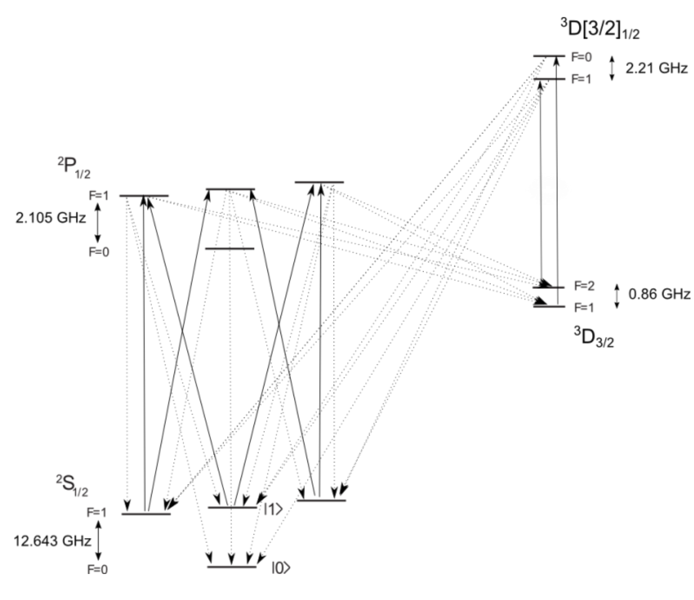

Figure 2.5: Qubit state initialization scheme for $^{171}Yb^+$

State initialization is accomplished by optically pumping the ^{171}Yb+ ion into the |0> state, as shown in Figure 2.5. During state initialization, the 369 nm beam with the positive 2.1 GHz sideband is used to drive the $^2S_{1/2}$ |F =1>↔$^2P_{1/2}$ |F=1> transition. From the $^2P_{1/2}$ |F=1> manifold, the ion has a 1/3 chance of decaying to |0>. Since $^2P_{1/2}$ |F=1>also decays to $^2D_{3/2}$ |F=2>, the aforementioned 3.07 GHz sideband in the 935.2 nm light is used for efficient state initialization. Thus, the ion eventually transitions to and remains in the |0> state. [21]

2.1.4 Hyperfine qubit control

Microwave radiation can coherently transition an ion initialized between |0> state and the |1> state. This is only possible on resonance when the energy of the microwave photon matches the energy splitting of the two hyperfine states. For an ion initialized to |0>, the probability P_0 (P_1) to find the ion in the |0> (|1>) state as a function of time is:

$$P_0 = \cos^2(\Omega_R t), \qquad P_1 = \sin^2(\Omega_R t)$$

where Ω_R is the Rabi frequency. Transitions from the |0> state to the |1> state are driven coherently with microwave photons near 12.643 GHz.

To provide this capability in the laboratory, a custom microwave pulse generation system was designed and constructed. The design is as follows: microwave electromagnetic fields are generated by mixing the signal from a fixed frequency dielectric resonant oscillator (DRO) at 12.600 GHz with that from a direct digital synthesizer (DDS) capable of tuning over a 300 MHz bandwidth using a microwave single-sideband mixer (SSB). Both sources are locked to a Rubidium vapor frequency reference at 10 MHz for superior frequency stability. The DDS frequency and phase are controlled by an FPGA controller configured for this task, as described in section 2.2. The FPGA also outputs synchronized TTL signals to a microwave switch for the generation of pulses. This signal is then delivered to a 2 W microwave amplifier. The amplified signal is delivered to the experiment by a microwave horn antenna. Ultimately, pulse sequences of up to three pulses with highly accurate pulse lengths, time delays, and phase relationship are delivered to the ion. The microwave hardware layout is illustrated in Figure 2.6.

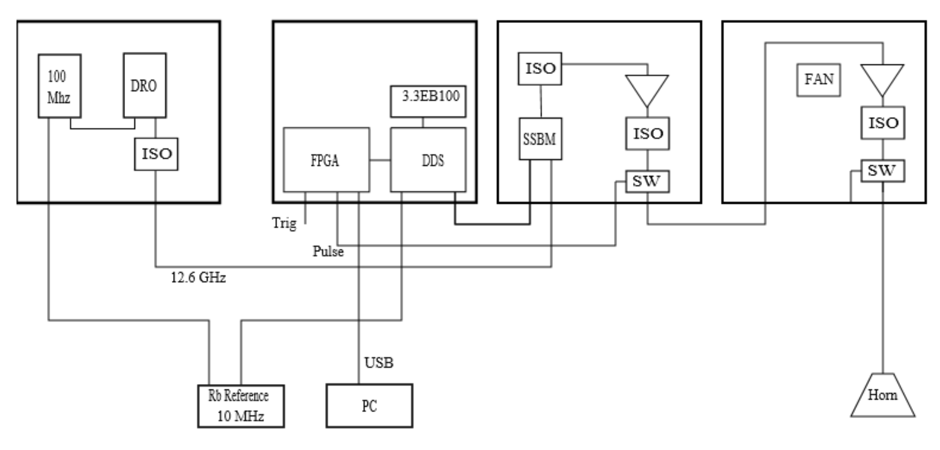

Figure 2.6: Schematic of microwave pulse control electronics

2.1.5 State detection

State detection is accomplished using standard ion fluorescence techniques, as illustrated in Figure 2.7. The 369.53 nm light of the detect beam is tuned to be nearly on resonance with the $^2S_{1/2}$ |F=1>↔$^2P_{1/2}$ |F=0> transition. If the ion is prepared in the state |0>, this incident light is detuned from the transition to the $^2P_{1/2}$ |F=1> state by 14.74 GHz, and thus the ion scatters very few photons. Conversely, if the |1> state is prepared, then the impinging light is nearly on resonance, and many scattered photons are observed. The state of the ion is determined by the number of photons observed by a deetector during the detection interval. [21]

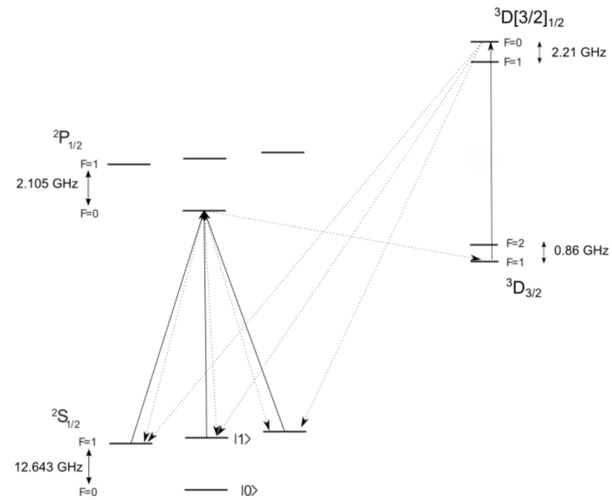

Figure 2.7: Detection scheme for $^{171}Yb^+$

2.2 Control electronics and software

Performing coherence experiments requires synchronization of ion control signals (including ion motion control in the trap), extremely precise electromagnetic field pulses in the optical and microwave frequency ranges, and data collection. To perform these functions, the above building blocks had to be integrated into a centralized control electronics system. The heart of the control electronics was the existing National Instruments based Digital Acquisition and Control (DAQC) system, in use for ion trap analog voltage control. There are four DAQC components pertinent to this section: analog output signals, digital output signals, a counter card for recording photon counter data, and a system control computer. The system is controlled from the CPU on board the DAQC chassis itself. This system was adapted and programmed to provide control of coherence experiments as described below.

Coherence experiments were programmed by control scripts in the scripting module of the DAQC control software on the system control computer. Control scripts were written in the Lua programming language, and two main types of scripts have been developed. First are lower level function scripts that perform waveform text file generation, equipment initialization (utilizing the LuaView interface and LabView instrument drivers), and data acquisition from either a camera or a photon-counter via the installed counter card. Second are high-level experiment execution scripts that coordinate experimental steps, in turn calling function scripts.

The user interfaces with the system through the scripting module, providing control parameters to the high-level control scripts. The user first indicates the waveform analog text file (shuttling file) to be referenced for ion motional control. These files are generated by modeling and simulation. The user then enters the overall experimental recipe broken down by operations (e.g., Doppler cool, shuttle, optically pump, apply microwaves, detect, and repump to the ground state). The times associated with these operations are determined by the script in various ways. For shuttling, the time is determined by the step time increment and number of steps included in the supplied text file. In the case of optical operations, operation times correspond to specified optical pulse lengths.

For microwave pulse sequences, the user enters pulse number and timing, pulse lengths, and phase, which are all passed to the microwave electronics component at initialization. The script determines a time for this operation to occur as a whole. The user also enters parameters for taking data, including bin size and number, which are passed to the installed counter card, and for performing iterations for statistics. Finally, because the experiments involve time or frequency scan data collection, the user enters the start, end, and step parameters for scanned data collection.

The main functions executed by the scripts are (1) merge user defined analog waveform files with digital control commands determined by user defined parameters into a synchronized combined analog/digital waveform file; (2) initialize the waveform chassis for waveform execution; (3) initialize experimental instruments including the microwave control FPGA, counter card for photon counting, and camera; (4) generate/execute the waveform, which outputs synchronized analog signals for ion positional control with digital trigger signals to the experimental equipment; (5) collect data; and (6) finalize/close equipment and de-allocate memory. Upon execution, the scripting module steps through these functions, according to the user-defined recipe, as described below.

The first function performed by the scripting module is generation of an integrated analog and digital waveform text file to synchronize ion motional control and instrument control. Ion motional control is provided by analog signals to electrode. Instrument control is provided by digital trigger signals to the AOM RF switches, microwave electronics component FPGA controller, camera, and the counter card. The control file lines are determined by merging the referenced analog control file and the user entered experimental recipe. All iterations within a coherence experiment begin with the ion in a stationary trapped and Doppler-cooled configuration. This is followed by stationary phases wherein electromagnetic control pulses are applied for coherent control interspersed with shuttle phases wherein the electromagnetic fields are switched off. The iteration terminates with a stationary phase where data is collected. The ion is ultimately returned to the statically trapped and Doppler-cooled configuration for the next iteration.

Given this experimental structure, the scripting module creates a control text file in the following way. The digital pulse sequence required for preparing the ion (Doppler cooling and state initialization) is determined from the user entered recipe and parameters. A low level functional script then replicates the first line of the analog file and appends the corresponding digital channel outputs at each step. If shuttling is directed by the user, the script then appends digital “off” signals to lines 2 through *N* (last analog line) and writes these lines to the integrated file. Finally, the script determines the measurement/data-taking and reset recipe, replicates line *N* accordingly, appends these recipe lines, and writes these lines to the integrated file. The result is a file with static analog signals while the preparation digital recipe is applied, followed by digital “off” signals while the analog shuttle recipe occurs, and then terminated with static analog lines again as the digital recipe controls data acquisition and reset. Further capability exists in the Ramsey spectroscopy script, where a spin-echo pulse may be inserted. This works in a very similar way with two identical shuttles performed sequentially with a stationary phase inserted between them in which a spin-echo microwave π pulse is accomplished.

After the waveform control file is generated, the waveform chassis is itself initialized for waveform execution, including allocation of memory, preparation for trigger activation, and required completion state. Additionally, the photon counter card and microwave FPGA are initialized and prepared for triggering.

Once all instruments are initialized and are in a prepared state for triggering, waveform execution is initiated by a trigger signal supplied by the scripting module. At this point, the scripting module waits for waveform completion and the waveform itself provides the execution control signals and serves as the timing reference. As the DAQC steps through the waveform, the lines are sequentially applied, applying synchronized analog and digital signals in accordance with the user-defined experimental recipe. Control of laser pulses is direct in the sense that the digital outputs are routed directly to the TTL inputs of the corresponding AOM power supply RF switches. The on-state of these signals directly determines pulse length and timing. The microwave electronics and photon counting components operate in a slightly different manner. Both these components are pre-loaded at initialization with their respective control programs. At the relevant part of the waveform recipe, the corresponding DAQC digital line serves to trigger this program. The associated program then runs autonomously for its specified duration while the waveform steps through a corresponding number of identical steps to maintain synchronization.

After execution of the waveform, the scripting module again assumes control of the experiment. Photon count data are recovered from the counting card and stored to memory in an array structure. Depending on the design of the experiment specified in the control script, the scripting module next performs an identical iteration of the recipe, appends data to the data array, steps to the next scan parameter and iterates, or proceeds to the finalization phase. In the finalization phase, the scripting module saves data array to a text file and resets the state of the waveform chassis, photon counting component, and microwave electronics component.

2.3 Coherent control scripts

In order for surface ion trap quantum information processing in microfabricated ion traps to be a viable technology, it must be demonstrated not only that the ions can be effectively trapped and shuttled in the required configurations, but also that their internal quantum states remain coherent during shuttling operations. Accomplishing this objective was addressed in the development of specific control scripts. These scripts synchronize the various CQO building blocks of (ion loading, state initialization, microwave qubit maniplation, and state detection). Scripts to perform coherent Rabi oscillations, Ramsey experiments, and Ramsey with spin-echo pulse experiments were developed and are described in the following sections.

2.3.1 Hyperfine resonance spectroscopy

Microwave radiation can coherently excite an ion initialized to the |0> state into the |1> state, and vice versa. This is only possible on resonance when the energy of the microwave photon matches the energy splitting of the two hyperfine states. For an ion initialized to |0>, the probability P_0 (P_1) to find the ion in the |0> (|1>) state as a function of time is:

$$P_0 = \cos^2(\Omega_R t), \qquad P_1 = \sin^2(\Omega_R t)$$

where Ω_R is the Rabi frequency. The observance of this sinusoidal behavior, or Rabi oscillations, of the hyperfine states constitutes a demonstration of a coherent operation on the qubit.

Matching the microwave photon energy to the energy splitting *E* of the hyperfine states correlates to matching the frequency *f* of the microwave radiation to the hyperfine splitting in frequency through the relation, *E=hf,* where h is Planck's constant. Providing resonant microwave radiation is nontrivial because the qubit states are magnetically sensitive and subject to a DC bias field. Therefore the resonant microwave frequency is shifted from its zero-field value. The energy levels shift according to the equation

$$E = g_F \, m_F \, \mu_B \, B$$

where g_F is the Lande factor, m_F is the magnetic quantum number, μ_B is the Bohr magneton (Planck's constant × 1.4 MHz/Gauss) and *B* is the magnetic field.

The first control task programmed was to accomplish microwave spectroscopy to search for the hyperfine resonance frequency, *f*. The control timing sequence is shown in Figure 2.8.

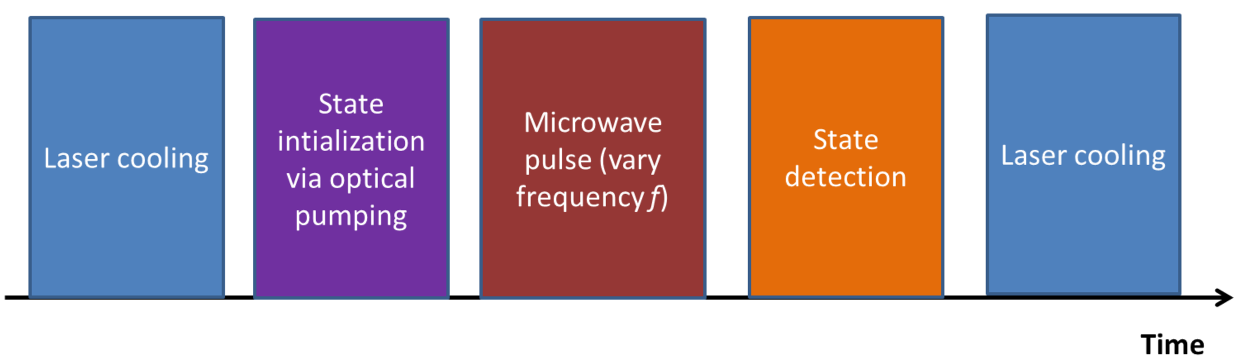

Figure 2.8: Experimental sequence to perform hyperfine resonance spectroscopy

The ion is trapped and laser cooled, then the qubit is initialized into the |0> state. This is immediately followed by a microwave pulse at frequency *f*. Photons are collected during a detection pulse to determine if the ion is observed in the |1> state after the pulse. This is repeated numerous times to develop statistics at each frequency in a band around the resonant frequency. The pulse time *t* is fixed. Ideally, a time corresponding to a (or an odd multiple of) half oscillation (π pulse) would be supplied to maximize population of the |1> state, giving the maximum signal. In practice, an estimate may be calculated, but trial and error must be employed if signal is not observed.

2.3.2 Rabi oscillations

A Rabi oscillation experiment is performed using the timing sequence shown in Figure 2.9. It is nearly identical to the spectroscopy sequence with the exception that the microwave pulse length is varied (on resonance) rather than varying the microwave frequency with fixed pulse length.

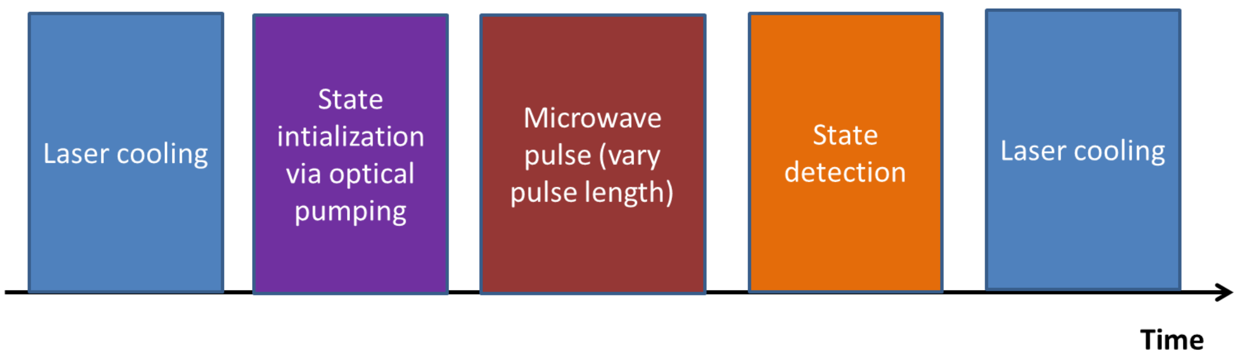

Figure 2.9 Timing for Rabi oscillation experiment

The qubit is initialized into the |0> state, immediately followed by a microwave pulse of variable length and a shelving sequence. Photons are collected during a 397-nm detection pulse to determine whether the ion remains in the |0> state after the microwave pulse. The signature of Rabi flopping is a sinusoidal variation of the photons collected during the detection pulse as a function of microwave pulse time. Decoherence time can be measured by fitting the data to a sinusoidal oscillation with an exponentially decaying envelope.

2.3.3 Ramsey experiment

Ramsey experiments are used to determine whether ion coherence is preserved during shuttling. Ramsey experiments are based on the same microwave resonance physics as Rabi oscillations and can only be performed after the Rabi frequency has been measured. The timing sequence is shown in Figure 2.10. After ion initialization, a microwave pulse satisfying $\pi/2 = \Omega_R t$, called a π/2 pulse, is introduced, which puts the ion into an equal superposition of |1> and |0>. After waiting a time (*T*), a second π/2 pulse is introduced with a phase (ϕ) relative to the first π/2 pulse. The probability to find the ion in the |0> and |1> state as a function of ϕ is

$$P_0 = \frac{1}{2}(1 - C\cos\varphi)$$

$$P_1 = \frac{1}{2}(1 + C\cos\varphi)$$

where *C*, the fringe contrast, is a coherence metric. As with the Rabi flopping experiments, state detection occurs after the Ramsey pulse sequence to measure the final state of the ion.

To demonstrate that coherence is maintained during shuttling in a surface ion trap, a Ramsey experiment can first be performed wherein the ion remains stationary during the wait time (*T*) in the Ramsey sequence (see Figure 1-3) and measuring the fringe contrast. The experiment is then repeated, but the ion is shuttled a distance (*d*) during *T* and the fringe contrast is compared with the Ramsey experiment where no shuttling was performed.

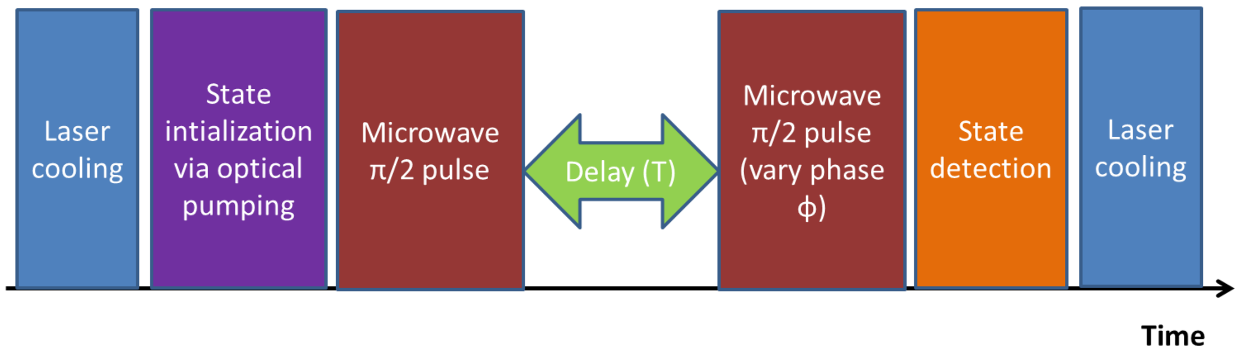

Figure 2.10: Microwave pulse sequence for a Ramsey Experiment

2.3.4 Ramsey experiment with spin-echo pulse

A Ramsey experiment with a spin echo pulse is very similar to the Ramsey experiment described above, but it slightly alters the microwave pulse sequence, as shown in Figure 2.11, to minimize the effect of time-varying magnetic fields.

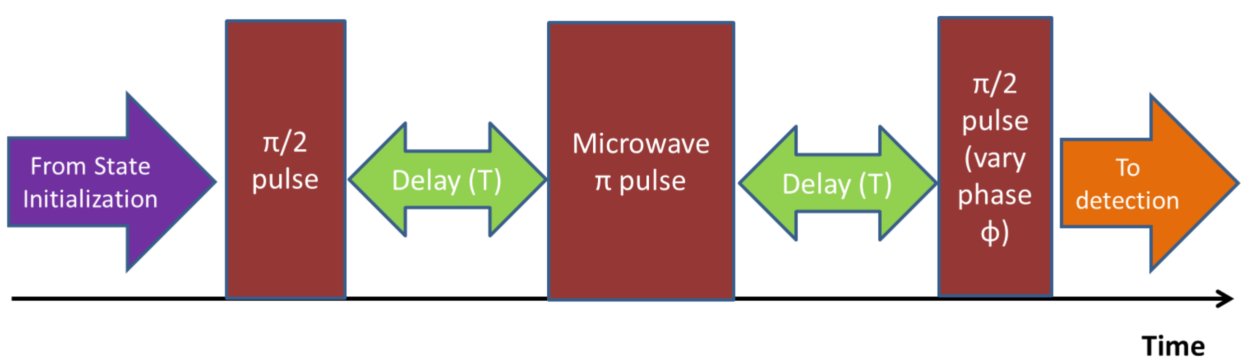

Figure 2.11: Microwave pulse sequence for a Ramsey Experiment with spin-echo pulse

The spin-echo sequence also begins with a $\pi/2$ pulse and ends with a second $\pi/2$ pulse with a phase ϕ relative to the first $\pi/2$ pulse. However, after the first $\pi/2$ pulse there occurs a wait time *T* followed by a microwave pulse satisfying $\pi = \Omega_R t$ (i.e., a π pulse) followed by a second wait time *T*. When the magnetic field is not perfectly controlled, the ion accumulates an uncontrolled phase between the two $\pi/2$ pulses. When many Ramsey experiments are averaged together, these uncontrolled phases amount to a washing out of the interference fringe. The π pulse in the spin-echo sequence ensures that any phase accumulated during the first *T* will be reversed during the second *T*. Therefore, the effect of the uncontrolled phase is negated and many experiments can be averaged together without washing out the fringe.

The probability to find the ion in the $|0>$ and $|1>$ state as a function of ϕ of the second $\pi/2$ pulse is identical to the expressions for P_0 and P_1 in the Ramsey experiment section. As with the Rabi flopping and Ramsey experiments, state detection occurs after the spin echo pulse sequence to measure the final state of the ion. Coherence during shuttling is demonstrated by first performing the spin-echo pulse experiment with a stationary ion, then repeating the experiment with the ion being shuttled a distance *d* during the both wait times *T* and verifying that the fringe contrast does not change.

2.3.5 Results and transition

The building blocks for performing coherence experiments with the $^{171}Yb^+$ ion at Sandia were developed under this project. Accomplishments included optical system design and implementation resulting in successful trapping of the $^{171}Yb^+$ ion in a microfabricated ion trap at Sandia. Additionally, a microwave control system was developed and the software to integrate the laboratory hardware for experimental control was developed. Ultimately, due to conflicting requirements, the coherent control capabilities were not utilized in this project, However, as a product of this work, these technologies enabled proposals for further ion trapping work and have been transitioned for use in other funded R & D projects at Sandia.

3 Device modeling and design

The device modeling and design effort of the project investigated the integration of microwave control elements with surface ion traps utilizing Sandia's state-of-the-art 4-metal-layer microfabrication process (Figure 3.1). The 4-metal-layer process is ideally suited because microwaves can be delivered by buried conductors in a stripline configuration with an overall top-side metal plane held at microwave ground. Interaction regions thus can involve local microwave electrodes; a top-side microwave ground plane covers the rest of the device, maximally shielding microwave fields from affecting other trap regions.

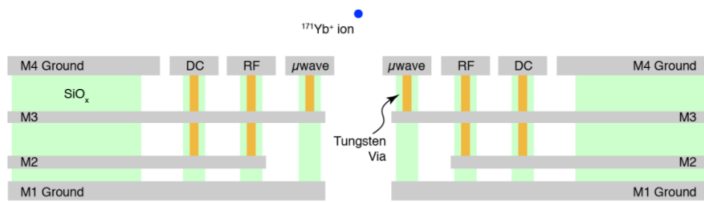

Figure 3.1: Metal routing and stack topology for multilayer trap fabrication – As shown on the right, microwave lines are routed under M4 ground on M3, up in vias through to M4, so stray fields do not result in decoherence. Long via sections are used so a weak spot in the line does not exist for power handling. Each metal layer is typically ~2.4 um thick

Initial design and modeling results pointed to ion traps with arrays of magnetic-field generating surface inductor coils as shown in Figure 3.2. The coil structures are desirable because they can generate large magnetic fields with a given current density. Additionally, the inductors generate magnetic dipole fields, which fall off very rapidly in the lateral dimension. This is an important feature because it reduces potential stray field cross-talk between envisioned trapping zones on a larger device. Note that, due to the topology of the structure, generating such structures requires multiple layer microfabrication technology. The simple configuration shown has four magnetic coils for the purpose of performing single qubit rotations and two qubit gates. Supplying different currents and phases to the coils controls the magnetic field in order to perform single qubit rotations or alternatively to cancel the field magnitude at the position of the ions while generating a finite magnetic field gradient in order to perform two qubit gates.

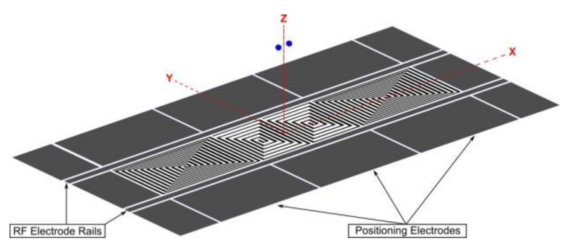

Figure 3.2: Schematic of preliminary microfabricated ion trap concept with zone for microwave two-qubit gate operations. RF electrodes create confining potentials in the Y and Z dimensions. Positioning electrodes create DC potentials that move the ions, join/separate them, and confine them in the X direction. Fields from microwave surface coils cancel at the position of the ions but generate a high field gradient for coupling to two-ion motional modes. The electrodes in this diagram measure approximately 100 μm on a side.

The initial concept also included using electrodes for multiple purposes. In this configuration, the coils can additionally be held at static voltages to serve as trapping electrodes and be supplied with DC current to set a local quantization axis. A further development would involve controlling the currents and phases of multiple coils to locally compensate for ambient fields or stray fields from neighboring interaction zones. Ultimately, devices with arrays of coils with multiple degrees of freedom are envisioned that could arbitrarily orient the quantization axis for different quantum gates and compensate for stray magnetic fields.

3.1 Coil array simulations

Preliminary simulations were accomplished with MATLAB to calculate the fields capable of being generated by simple surface coil structures using a DC approximation. These preliminary results indicated that a field gradient of ~ 30 Tesla/m could be generated in both the X and Y axis directions at an ion height of 40 µm above the surface. This gradient is comparable to the value achieved by the NIST group in performing two-qubit operations.[16]

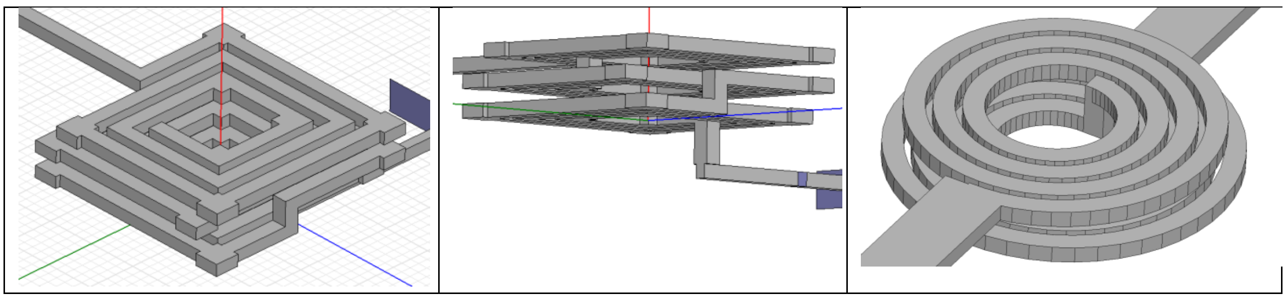

Figure 3.3: Multi-turn, multi-layered inductor structures examined for magnetic field strength. Width of each inductor electrode is 3 um.

More sophisticated simulations were then carried out to model the fields produced by three dimensional coil structures and arrays achievable with the Sandia 4-metal-layer process. These simulations were accomplished using the Ansys HFSS software package, a commercial finite element method solver for electromagnetic structures. The fabrication process allows for 4 layers of 2.4 um thick metal, and a total of 15 um of oxide to separate these layers. The first structures simulated were single and multi-layer inductor structures, as shown in Figure 3.3.

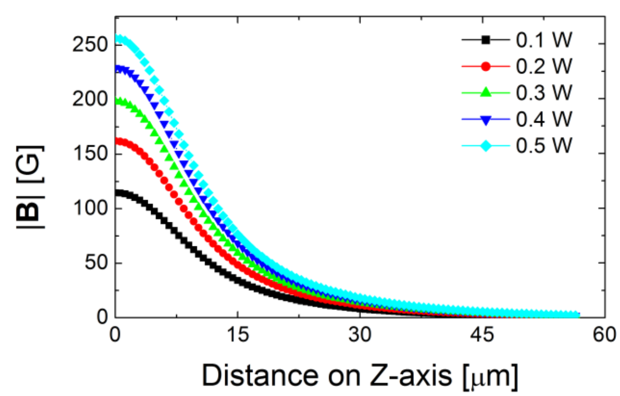

Figure 3.4: Magnetic field strength vs. height on the z-axis for several power levels for a single inductor with 60um lateral dimension. Field strength drops off significantly as a function of height.

Initial simulations calculated the on axis magnetic field strength achievable with these types of structures with nominal power levels, as seen in Figure 3.4. The coils structures are capable of creating quite significant field strength. However, it can be seen that the field strength drops off significantly as a function of height on the order of inductor dimension. This is problematic for the initial design concept because coil diameter is constrained between the RF rails, which dimension in turn determines the ion height. Increasing coil diameter in this design thus also raises ion height, counteracting the gain in field strength. The nominal height of an ion in a typical Sandia microfabricated trap is approximately 40 µm.

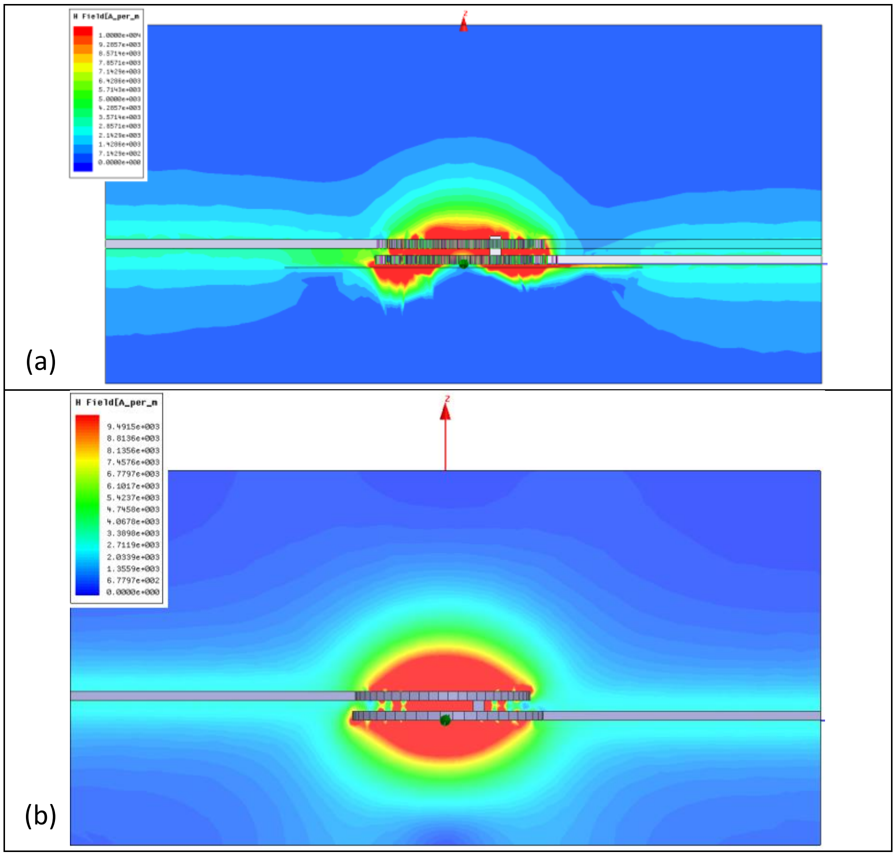

Figure 3.5: Magnetic field density both (a) with and (b) without a ground plane beneath the inductor. The ground plane represents the lossy silicon substrate. Metal trace width is 2.4 um.

Because the fabrication process normally introduces a ground plain below the inductor, the effect on field strength of such a ground plain was also studied, as seen in Figure 3.5. The ground plane reduces fields above by almost an order of magnitude. One possible mitigation approach at Sandia is to remove the substrate under the coils, although this poses an additional fabrication risk. The substrate used is a conductive silicon wafer, which acts as a ground plane. Image currents generated in the substrate result in a lower magnetic field. This is especially true as distance from the substrate (ion height) increases. As a result, one strong consideration in fabrication is to remove the substrate from beneath the inductor structures. This would reduce the effect of the substrate on generating magnetic fields, but has the potential to increase fabrication risk and decrease yield. Another possible solution is to use an insulating substrate, such as high-resistivity silicon (>10,000 ohm-cm) and removal of M1 ground plane beneath structures.

A further capability addressed by the design is to perform two qubit operations with microwave magnetic fields. For the purpose of performing two qubit gates, it is desired to cancel the field at the ion while maintaining a large field gradient.[9] This involves supplying magnetic field gradients on the order of 10 T/m while minimizing field magnitude at the position of the ions in order to avoid unwanted single qubit rotations (*carrier* transitions). Simulations were conducted to study this capability in the coil array architecture as seen in the figures Figure 3.6 and Figure 3.7.

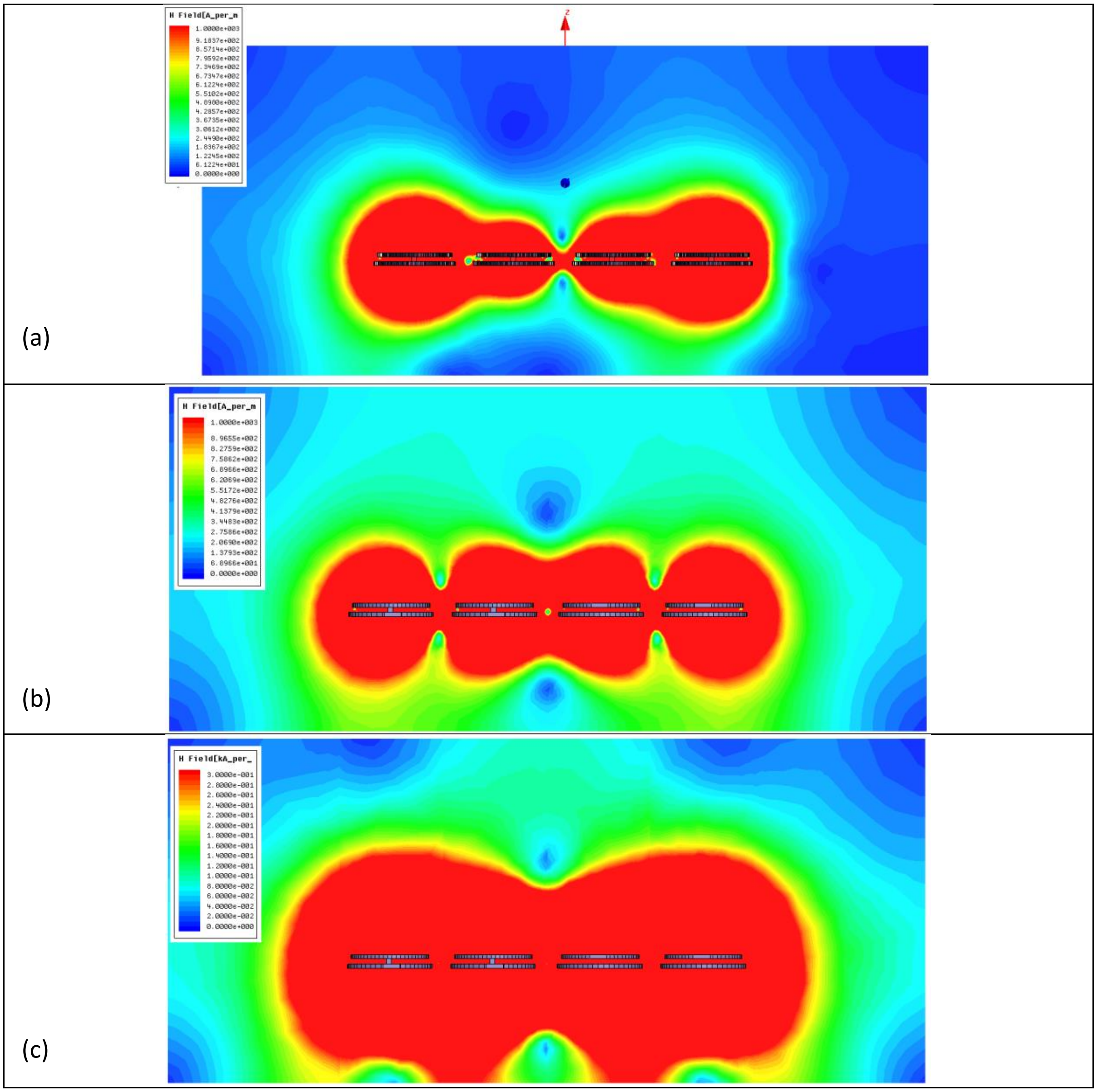

Figure 3.6: (a) First attempt at creating a null by using multiple inductors. The microwaves are fed through the inductors with equal amplitude. The turn directions and phases of the feeds equate to 0,180,180,0 phase angles, allowing for cancellation at the center. Power levels and phases in each coil were then modified to generate (b) lower and (c) higher nulls. These can be used for ions or traps with various heights.

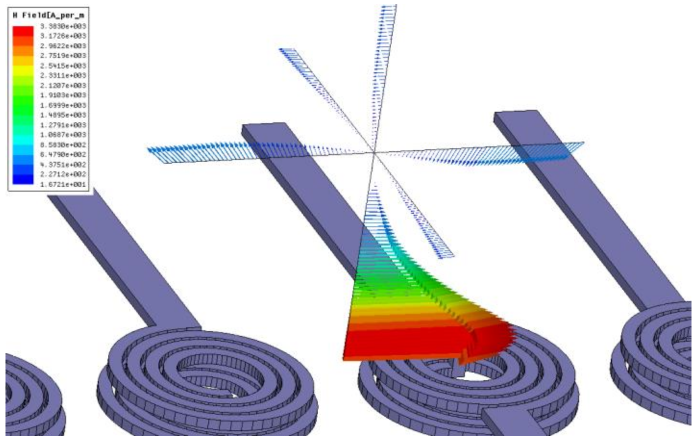

Figure 3.7: Graphic showing magnetic field on lines through ion location. Large magnetic fields exist in the X-direction along the Z-axis, along the Z-direction in the x-axis, and along the x-direction in the y-axis. However, these are all cancelled at the ion location.

With the magnetic field necessary to generate such a field gradient, the microwaves are relatively high power. As a result, there are tradeoffs between number of turns, metal width, and power to be considered. Figure 3.8 shows the approximate surface current density of the inductor for a given input power level. Three issues of concern involving high powered signals are electro-migration, thermal issues, and burning out individual traces. Electro-migration is typically a problem at DC, and arises when current densities exceed 50 kA/cm^2. At microwave frequencies this is typically less of a problem, but can still be an issue, as the skin depth is smaller than the actual trace size. The second issue is thermal problems. The metal layers have thick oxide and air gaps, resulting in a very poor thermal conductivity, and very low thermal time constant. Therefore, even for pulse-based systems of around 1ms, the device will approach thermal steady-state. For this reason, thermal concerns are one of the major design concerns. In addition, the trace will only be able to carry as much as its smallest section, so proper heat-sinking and creating wide traces are issues of concern.

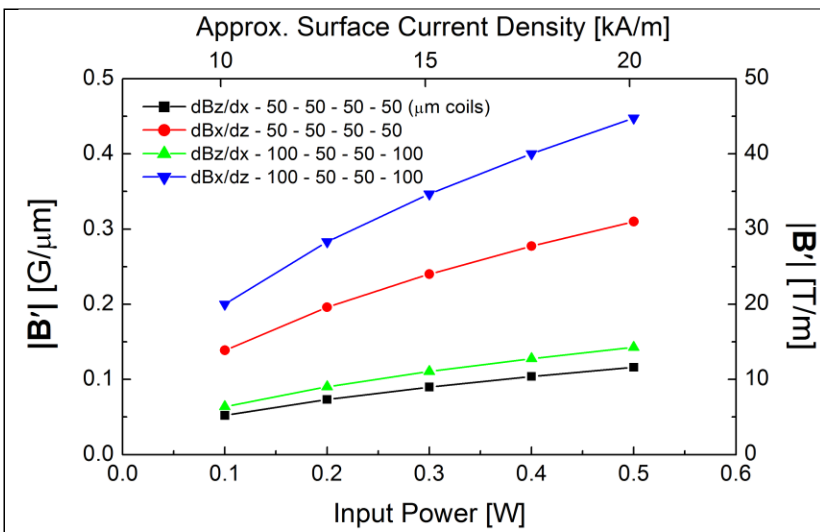

Figure 3.8: Gradient created versus input power, highlighting approximate surface current density.

3.2 Concentric-coil / parallel-line architecture

After simulations of the first variations with lateral coil arrays, it was determined that it would not be the optimal approach for several reasons. First, to avoid carrier rotations, it is optimal to minimize the magnetic field magnitude along a line segment containing both ions for a two qubit gate. Second, because the inner coils must fit between the RF rails (which spacing determines ion height), the lateral dimension of these coils would be too small to produce adequate fields at the ion. Third, the small traces on the inductors are difficult to fabricate with supports, and they will have a lower maximum input power than the rest of the structure.

An alternative solution was investigated to instead utilize concentric inductors to generate the desired field gradient along the vertical axis with null field amplitude along the longitudinal trap axis. As a simple model, two concentric inductors can be used to generate the desired field. For two simple concentric circular inductors, with radii R_1 and R_2, the following equation can be solved for a given vertical position z:

$$B = [\frac{\mu I_1 {R_1}^2}{2({R_1}^2 + z^2)^{3/2}} - \frac{\mu I_2 {R_2}^2}{2({R_2}^2 + z^2)^{3/2}}] = 0 \quad .$$

This results in a specific external radius for a given ratio of currents, or a specific ratio of currents for a given external radius. When this geometry is then extended along the longitudinal trap axis, it results in an extended field null along the longitudinal axis experienced by both ions with a finite gradient along the vertical axis. Additionally, the ends of the inductors can be routed under the surface. The extended inductor then appears to the ion as a set of longitudinal wires. In practice, of course, it is not necessary (or desirable) to connect the wires into coils as long as phase is correctly controlled.

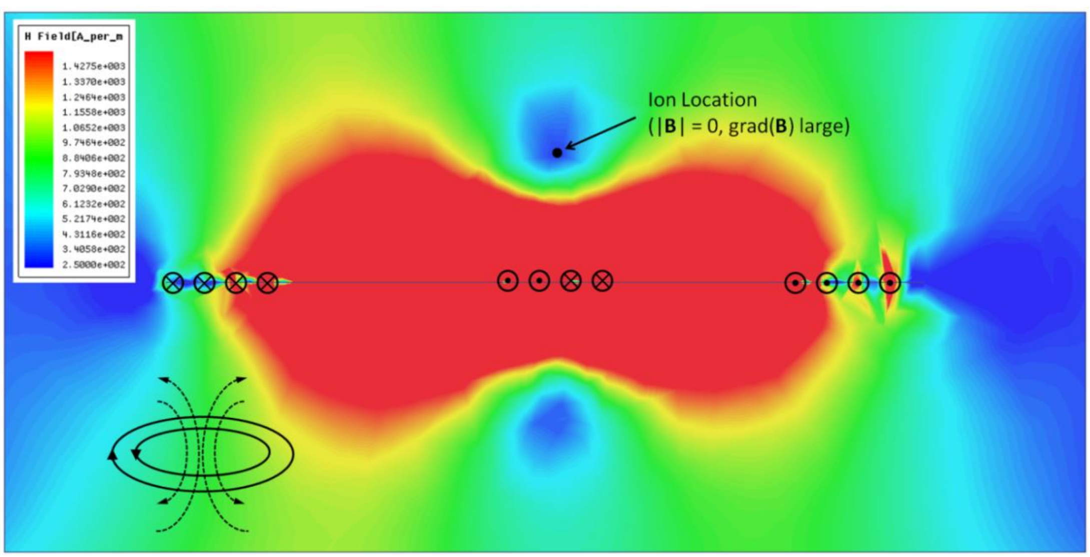

Figure 3.9: Two external coils and one internal coil with current direction labels. The inner set of wires represents one inductor, and the outer two sets represent another inductor.

The effects of inductor dimensions on field gradient and null position (ion height) were also simulated as seen in Figure 3.10 and Figure 3.11. Because each line can be fairly wide, the maximum power handling of this device is higher than small-turn inductors. Test devices would determine how much power these can handle, but typical RF lines have no problem handling several watts of power. The limiting constraint in this case will likely be thermal effects from long-time operation instead of power handling of the individual traces. The traces are routed through vias as shown in Figure 3.1. The vias used are long sections designed to be an equivalent width to the trace, so that a weak point does not exist for power handling.

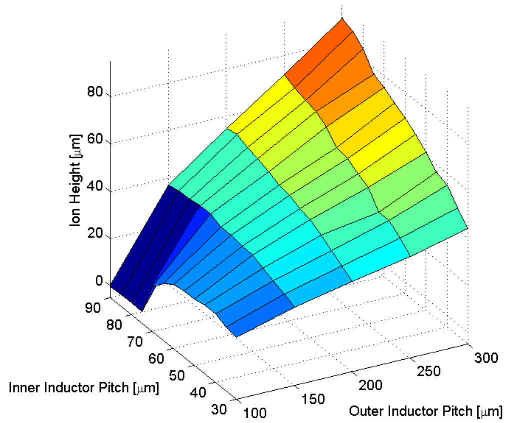

Figure 3.10: Ion Height as a function of inner and outer inductor size. If a certain ion height is desired, the line caused by the intersection of this plane with the specific height can be chosen for inductor sizes.

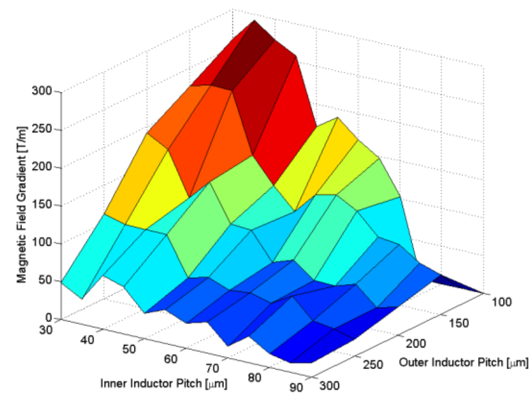

Figure 3.11: Magnetic field gradient versus inner and outer inductor pitch. The gradients listed here are normalized to 1W input on each inductor. It is unlikely that the trap can handle 1W in CW operation, so these numbers should be scaled based on current handling capability.

Using this topology, the ion height and magnetic field gradient were determined for varying inner and outer inductor outer diameters. This is done because once an ion's height is determined, the user can easily check these plots to see what inductor sizes are necessary, and if a sufficient gradient can be achieved at this level.

3.3 Off-chip matching

Because a matching network on-chip would take up valuable chip real estate and might not take into account unforeseen parasitics, the microwave matching network will be done off-chip. With this method, we can make each line as wide as reasonable, simply measure the input impedance of the line after fabrication, and design the matching network around it. This matching network can easily be designed into the (likely ceramic) interposer which will provide the DC and RF feed lines. The matching technique used will be a single stub match. This is a simple, effective, but narrowband technique, but since we have a narrowband microwave signal, it is inconsequential. With matches such as these, an almost perfect match can be generated at a narrow set of frequencies.

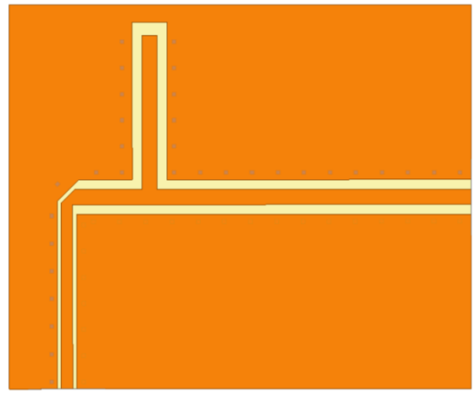

Figure 3.12: Example of RF board coplanar waveguide (CPW) line with single stub matching network - The matched frequency is determined by the length of the stub and the distance the stub is from the load. These are typically narrowband, but we do not need a broadband match in this case.

3.4 Trap design

The ultimate vision developed in this project is a microfabricated ion trap architecture with multiple control zones, each with multiple degrees of freedom for controlling to perform various operations with solely electronic control. The concept includes new concepts to deliver multiple microwave signals to the chip, including utilizing combined signals across a broad bandwidth ranging from DC to microwave frequencies, in order to use the electrodes for multiple functions. The ultimate design concept must accomplish several functions such as setting the DC magnetic field (quantization axis) along any direction to enable arbitrary single qubit rotations, setting DC magnetic field gradients for individual ion addressing (by position dependent Zeeman shifts), providing large magnitude microwave magnetic field pulses for fast single qubit rotation, supplying a high magnetic field gradient with a minimum field amplitude for performing two qubit gates, and simultaneously reducing compensating for cross-talk fields between zones.

Toward this vision, a first design of a surface ion trap capable of local on-chip microwave qubit control was developed. The device consists of two similar ion traps arranged in parallel (see Figure 3.13 for top metal layout and Figure 3.14 for trap detail). The ion traps are based on existing linear traps at Sandia. The unique feature is a set of electrodes for microwave field generation based on the simulations discussed in section 3.2. The trap-design emphasizes efficient routing of microwave pulses to ion trap zones with maximal shielding of stray fields, utilizing buried microwave leads and surface field generating elements. Such elements require via interconnects between metal layers and trap structures that span multiple layers in order to minimize current density while maximizing field and/or gradient strength. A framework for routing and distributing the microwave lines to ion interaction zones was developed within the parameters of the existing fabrication process. The microwave electrodes are connected by tungsten vias to microwave transmission lines beneath a surface metal layer designed to be a microwave ground shield. Additionally, the device was designed with the ground plane (substrate) removed beneath the microwave electrodes for greater field generation.

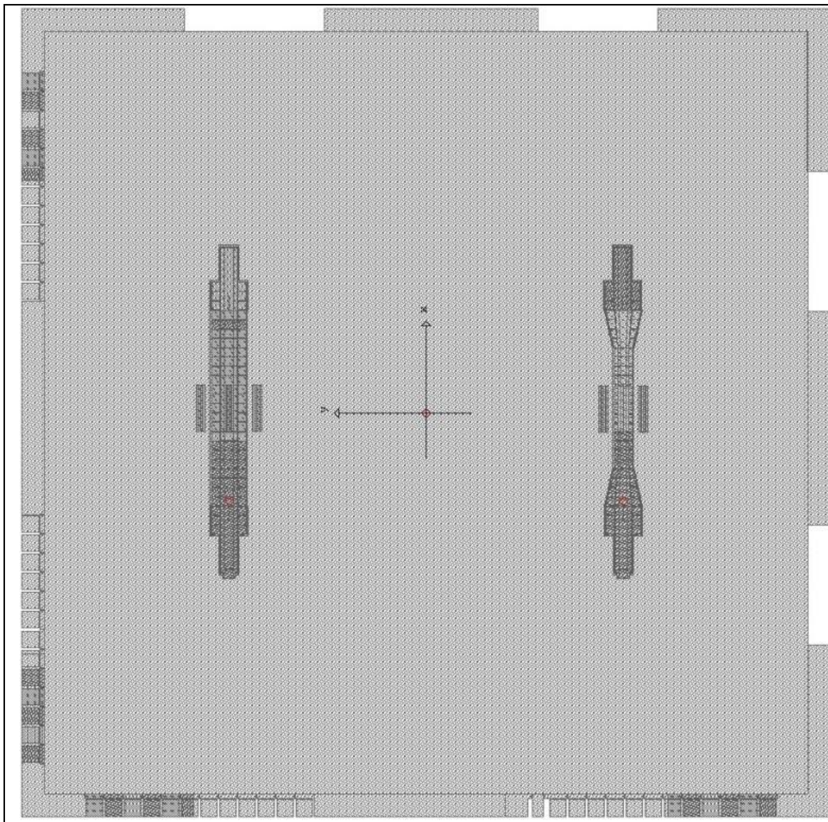

Figure 3.13: Top metal layout for two trap test device with intervening microwave shield. Note that all electrodes are connected with leads buried beneath the top metal layer.

The device is designed as a test platform for investigation of a number of these technologies. The device is designed to enable the following demonstrations/experiments:

1. On-chip controlled fast single qubit rotations
2. Device coherence time characterization (Ramsey experiment)
3. Device coherence time measurement with shuttling
4. Local control of quantization axis
5. Cross-talk characterization between control zones separated by a top-metal shield
6. One dimensional cross-talk compensation experiments between separated control zones
7. On-chip controlled two qubit coherent operations
8. Ion height variation with shuttling
9. Effect of ion height on above coherent operations

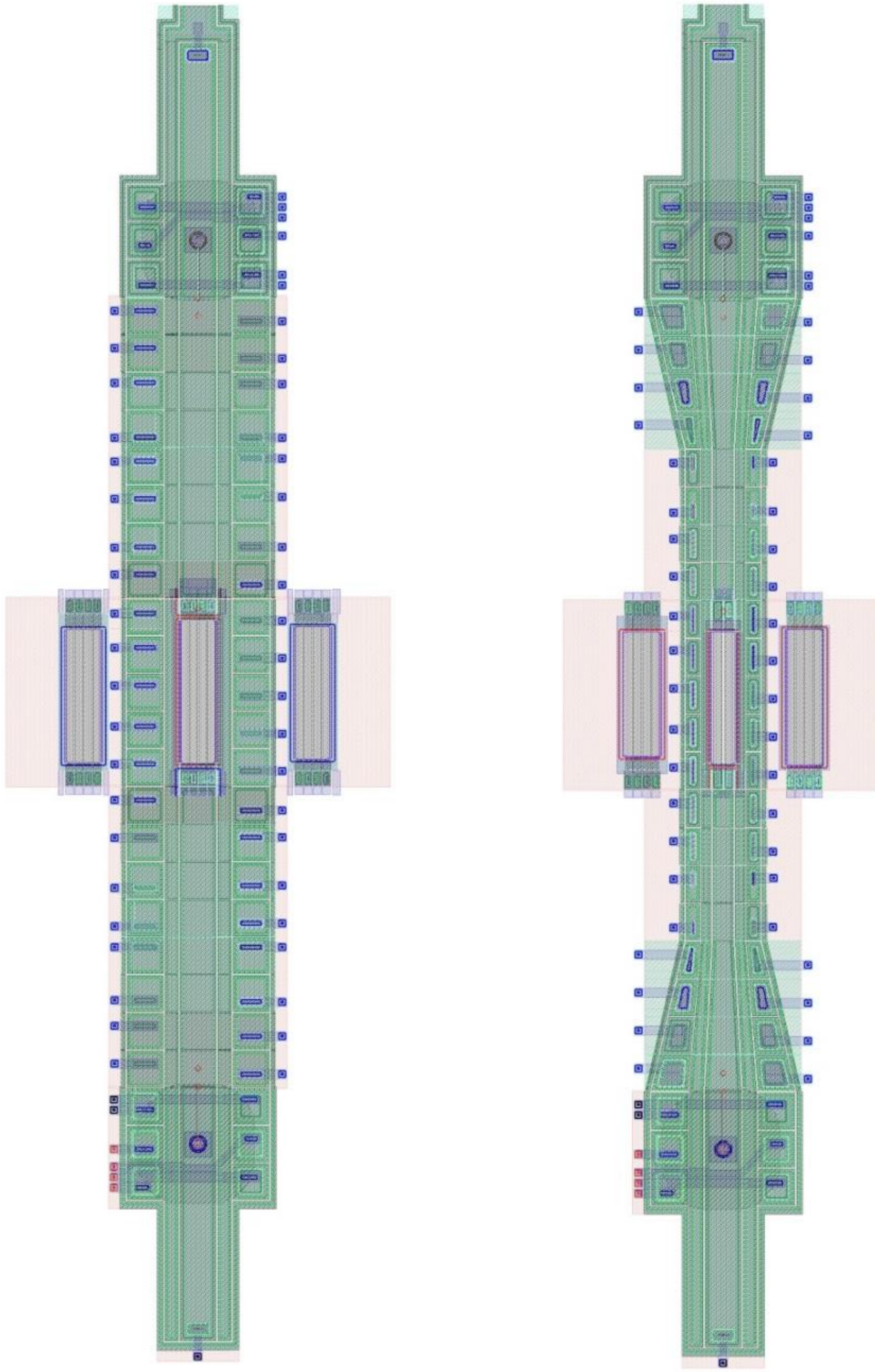

Figure 3.14: Ion trap designs for investigation of on-chip microwave ion qubit control. The designs capitalize on existing four metal layer microfabrication capability to deliver microwaves by buried stripline leads to (3) local surface electrodes centered on the interaction zones at the trap centers. Additionally, the grounding substrate is removed beneath the microwave electrodes (suspended electrodes) to enhance field generation. The trap on the right is designed to investigate the capability and effects of lowering ion height in the interaction zone.

4 Transition and way forward

The most significant question that remains is whether the achievable current densities in the microfabricated devices will be sufficient to generate the desired magnetic fields. This is almost certain for fast single qubit operations. However, the fields required to produce gradients for practical two qubit operations are very high. Initial results from this work are promising, but a more comprehensive design study is warranted, as is a specifically focused experimental effort.

More research into geometric layout could provide beneficial solutions. Furthermore, since the limiting factor identified in this work is resistive Joule heating in microwave leads, mitigation of this risk could involve development of enhanced conductivity leads through cryogenic operation. This would involve a reasonable and valuable investment in laboratory capability. At liquid nitrogen temperature (77 K), the conductivity of aluminum is higher by an order of magnitude than at room temperature. This conductivity improvement results in a significant increase in available current density. Liquid nitrogen is inexpensive and relatively easy to implement and has a high heat capacity required for thermal management.

At liquid helium temperature (4.2 K), the conductivity of aluminum is higher by four orders of magnitude than at room temperature, which could provide substantial gains. Another alternative is to incorporate niobium (Nb) metallization into the ion-trap microfabrication process. Niobium is a superconductor with T_c = 9.15 K which enables superconducting operation at liquid helium temperature. Niobium processing is currently available in Sandia's MESA facility and has been verified to produce superconducting electrodes. However, with either helium option, thermal management could be problematic and energy transfer would need to be studied.

Future development would involve fabrication of the ion trap test platform device design. Additionally, a custom electronic interface would need to be developed in the laboratory to deliver microwaves into an ultra-high vacuum chamber. The laboratory systems developed under this program would first be used to demonstrate on-chip microwave control with single qubit rotations. A research goal here would be to generate high magnetic fields at the ion and accomplish high speed operations. Another important result would be to use the developed systems and control software to characterize the coherence maintaining capability in the traps, both statically and with ion shuttling.

Additionally, the cross-talk between interaction zones could be characterized and experiments could be accomplished to investigate compensation of cross-talk between zones separated in one dimension. The design incorporates two separated interaction zones for simultaneous operation, separated in one dimension for simplicity. For cross-talk characterization, a test ion is trapped and shuttled to a an interaction zone and prepared in an initial quantum state. A microwave single qubit rotation pulse corresponding to a finite rotation angle is then be sent to the distant zone and the local effect on the test ion is measured. The effect on the test ion will be a deviation from the initial state equivalent to a Bloch sphere rotation of the state vector on some axis through an angle less than that associated with distant pulse. This error will be analyzed in terms of the unintended test ion rotation angle relative to the distant zone intended rotation angle.

Once that cross-talk effect is characterized, a further experiment would be cross-talk compensation. This involves locally compensating the error due to distant applied pulses. Further work could build on extensive tools developed at Sandia for electrostatic modeling and control solution calculations. Simulation would be used to develop control techniques for compensating cross-talk effects. Since Sandia's approach also tightly links modeling and simulation with experimental testing and implementation, an experimental effort would concentrate on the capability to generate compensation signals simultaneously with control signals and implementing them to minimize cross-talk effects.

Finally, as resources permit, the multipurpose traps can be implemented to first perform two qubit operations and then demonstrate multiple functions within a single trap zone. These functions include setting the DC magnetic field quantization axis along any direction to enable arbitrary single qubit rotations, setting DC magnetic field gradients for individual ion addressing (by position dependent Zeeman shifts), providing large magnitude microwave magnetic field pulses for fast single qubit rotation, supplying a high magnetic field gradient with a minimum field amplitude for performing two qubit gates, and simultaneously compensating for cross-talk fields from other zones. Finally, the effects of varied ion height on these operations can be studied.

Overall, this project developed expertise and capabilities at Sandia toward on-chip, localized, and laser-less qubit operations in a scalable architecture. The project developed a foundation of basic building blocks, including laboratory capabilities for hyperfine ion qubit trapping, coherent control, and experimentation. Additionally, the project investigated the integration of simple microwave device elements with surface ion traps utilizing Sandia's state-of-the-art MEMS microfabrication processing. This effort culminated in a device design for a multi-purpose ion trap experimental platform for investigating on-chip microwave qubit control. Overall, this work has laid the groundwork for further funded R&D to develop on-chip microwave qubit control in an architecture that is suitable to engineering development.

References

[1] D. J. Wineland, Physica Scripta T137 (2009)

[2] R. Blatt and D. Wineland, Nature 453, 1008 (2008)

[3] M. Nielsen and I. Chuang, Quantum Computation and Quantum Information (Cambridge University Press, Cambridge, 2000)

[4] D. Leibfried et al., Reviews of Modern Physics 75, 281 (2003)

[5] D. J. Wineland et al., J Res Natl Inst Stan 103, 259 (1998)

[6] J. I. Cirac and P. Zoller, Physical Review Letters 74, 4091 (1995)

[7] D. Kielpinski, C. Monroe, and D. J. Wineland, Nature 417, 709 (2002)

[8] F. Mintert and C. Wunderlich, Physical Review Letters 87 (2001)

[9] C. Ospelkaus et al., Physical Review Letters 101 (2008)

[10] J. Chiaverini and W. E. Lybarger, Physical Review A 77 (2008)

[11] A. M. Steane, Quantum Information & Computation 7, 171 (2007)

[12] R. Ozeri et al., Physical Review A 75 (2007)

[13] M. Johanning et al., Physical Review Letters 102 (2009)

[14] S. X. Wang et al., Applied Physics Letters 94 (2009)

[15] C. Ospelkaus et al., arXiv:1104.3573v3 [quant-ph] (2011)

[16] K. R. Brown et al., arXiv:1104.2552v1 [quant-ph] (2011)

[17] D. Stick et al., arXiv:1008.0990v2 [physics.ins-det] (2010)

[18] D. L. Moehring et al., New Journal of Physics 13 (2011)

[19] G. R. Brady et al., Applied Physics B-Lasers and Optics 103, 801 (2011)

[20] D. T. C. Allcock et al., arXiv:1105.4864v1 [quant-ph] (2011)

[21] S. Olmschenk et al., Physical Review A 76 (2007)

Distribution

1	MS0899	Technical Library	9536 (electronic copy)
1	MS1082	M. Descour	1725
1	MS0359	D. Chavez, LDRD Office	1911
5	MS1248	C. Highstrete	5643
1	MS1248	S. Rinaldi	5643

Sandia National Laboratories